Supplementary Information

Sample Description and Two-Pyroxene Temperature

Petit-spots have been successively discovered from many sites in the world (Japan Trench: Hirano et al., 2006; Tonga Trench: Hirano et al., 2008; Basin & Range: Valentine and Hirano, 2010; South of Greenland: Uenzelmann-Neben et al., 2012; Chile Trench: Hirano et al., 2013; Northeast Indian Ocean: Taneja et al., 2014). From petit-spot volcanoes on subducting Pacific Plate off the Japan Trench (Fig. DR1) about a dozen peridotite xenoliths have been identified in so far collected petit-spot basalts (Yamamoto et al., 2009), but most of them are smaller than 1 cm in diameter. The peridotite xenoliths used in this study are relatively large (> 2 cm diameter) and are spinel lherzolites except for sample 2Aa, which is lherzolite not showing any aluminum-dominated mineral such as spinel, garnet, and plagioclase. All the peridotite xenoliths show a porphyroclastic to equigranular texture. The constituent minerals largely have around 1 mm diameter average size. These xenoliths have already been analyzed for major elements and noble gas isotopes (Yamamoto et al., 2009). Slightly high Fo values ([Mg / (Mg + Fe) × 100] of olivine) and Cr# [Cr / (Cr + Al) × 100] of spinel suggest that these peridotites were derived from mantle sources that had been slightly melted.

Yamamoto et al. (2009) reported the temperature determined using a two-pyroxene geothermometer. Sample 2Al shows relatively high uncertainty of 846 ± 88°C. In order to identify the cause of the uncertainty, we reanalyzed the major element composition of all samples. We listed the major element composition of the core and rim parts of minerals (Tables DR1 and DR2). Except for sample 2Al, there is no significant difference between core and rim compositions. Clinopyroxene of sample 2Al shows heterogeneous compositions of CaO and Na_2O resulting in a huge uncertainty of temperature of rim part (802 ± 151°C: Table DR2). We obtained temperature of 771 ± 58°C from core part of the sample 2Al, which is unexceptionally tight uncertainty for peridotites, and similar to uncertainties of the other samples (30–55°C: Table DR1). Thus the relatively large uncertainty of sample 2Al is possibly due to intense reaction with host magma. Such chemical zonation was not observed in the other samples.
It is important to evaluate the equilibrium conditions of the minerals in a peridotite xenolith when applying a thermodynamical geothermometer. Putirka (2008) examined a set of 311 experimental pyroxene pairs, and obtained a Fe-Mg exchange coefficient between clinopyroxene and orthopyroxene, which is defined as

$$K_D(\text{Fe-Mg})^{\text{cpx-opx}} = (X^{cpx}_{Fe}/X^{cpx}_{Mg})/(X^{opx}_{Fe}/X^{opx}_{Mg})$$

where X^j_i refers to the mole fraction of component *i* in phase *j*. By discarding the data outside of 3σ bound, the $K_D(Fe\text{-}Mg)^{cpx\text{-}opx}$ of 1.09 ± 0.14 has been proposed to evaluate the equilibrium condition of two-pyroxene. The $K_D(Fe\text{-}Mg)^{cpx\text{-}opx}$ of the present xenoliths are listed in Tables DR1 and DR2. The $K_D(Fe\text{-}Mg)^{cpx\text{-}opx}$ of samples 2Al (0.77–0.78) and 2Aa (0.57) are quite beyond the proposed range, implying that the uncertainties of two-pyroxene temperatures of both samples are large. The $K_D(Fe\text{-}Mg)^{cpx\text{-}opx}$ of sample 2D (1.07–1.08) is analogous to the proposed value. On the other hand, taking careful selection of data by Putirka (2008) into consideration, the $K_D(Fe\text{-}Mg)^{cpx\text{-}opx}$ of sample 2As (0.91–0.93) is within the range of the proposed value. Thus at least two xenoliths (2D and 2As) are adequate to estimate two-pyroxene temperatures.

Analytical Procedures for Micro-Raman Spectroscopy

Precise determination of CO_2 density of fluid inclusions is essential for the estimate of depth provenance of the peridotite xenoliths. We followed the analytical procedures for density measurements proposed by Yamamoto and Kagi (2008). The samples were sliced into thin (ca. 300-μm-thick) slabs, doubly polished, and mounted on glass slides. Raman spectra of CO_2 inclusions were obtained using a 30-cm single polychromator (250is; Chromex) installed at Geochemical Research Center, University of Tokyo, which is equipped with an optical microscope (BX60; Olympus Optical Co. Ltd.), Ar ion laser (550A; Ion Laser Technology, Inc.), and a CCD camera with 1024 × 128 pixel resolution (DU-401-BR-DD; Andor Technology). The intense Rayleigh line was removed using a holographic filter (super-notch-plus, HSPF-513.3-1.0; Kaiser Optical Systems, Inc.). An excitation laser beam of 514.5 nm wavelength was focused on spots of 1 or 2 μm diameter respectively using a ×100 or ×50 objective lens (Olympus Optical Co. Ltd.). Consequently, the laser power on the sample surface was 20 mW. The spectral resolution in the present system is approximately 1.5 cm^{-1}, but that resolution can be enhanced to 0.03 cm^{-1} by application of a curve fitting technique (Kawakami et al., 2003; Fukura et al., 2006). More than 500 counts of the Fermi diad band at 1388 cm^{-1} are necessary to obtain a delta value with high resolution (within 1σ of 0.03 cm^{-1}) for the present system (Kawakami et al., 2003). Spectra were accumulated for 300–900 seconds to obtain high signal counts.

Purity Test of Fluid Inclusions

Almost all minerals in the peridotite xenoliths have fluid inclusions with negative crystal shape (Fig. DR2). Depth provenance of the xenoliths was estimated using residual pressure of the fluid inclusions, which have no association with crack or melt inclusions as shown in Fig. DR2. Berkesi et al. (2009) reported that Raman spectroscopic analysis at high temperature (~150°C) is effective to detect small amount of H_2O in CO_2-rich fluid inclusions. The occurrence of water influences the equation of state of fluid, which is used to calculate the depth provenance of the xenoliths. We performed the high temperature Raman analysis of the fluid inclusions. As shown

in Fig. DR3, no water can be detected from the fluid inclusions in all the peridotite xenoliths even at 150°C. We can safely say that the fluid inclusions are entirely dominated by CO_2 fluid.

Accuracy in Depth Provenance of the Peridotite Xenoliths

The depth provenance of a peridotite xenolith is usually estimated by using the pressure dependence of pyrope breakdown reaction into orthopyroxene solid solution, but unfortunately no garnet is found in our xenoliths. Köhler and Brey (1990) proposed a geobarometer applicable to a garnet-free peridotite using partition of Ca between olivine and clinopyroxene. We tried to calculate the equilibrium pressure of the present xenoliths by applying the geobarometer (KB90) to the core compositions of minerals. The high-precision analysis of Ca in olivine was conducted using an electron microprobe (JXA-8900, JEOL) with an accelerating voltage of 25 kV and a beam current of 20 nA. We obtained peak intensity of Ca (Kα) of 3000–14000 counts from the present olivine grains. The precision of the intensity of Ca is around ± 2% (1σ) at 3000 counts, corresponding to ±4 ppm at 200 ppm Ca. The averaged CaO contents of core part of olivine grains in samples 2As, 2Al, 2Aa, and 2D were, respectively, 374 ± 26, 167 ± 29, 231 ± 35, and 880 ± 62 ppm. The obtained pressures (Table DR3) are scattered and characterized by substantial uncertainties, and they do not show correlation with temperature. Furthermore some xenoliths are assigned with unrealistic pressure as spinel peridotites, which are stable in mantle at 1.0–2.2 GPa (Table DR3). Taking the lower end of prediction, the KB90 pressure of sample 2As can be marginally compatible with the spinel stability field, but that of sample 2Aa is still far above the stability field.

Here it is worth describing in some detail how we determined the uncertainty of the KB90 geobarometer. The KB90 geobarometer is given by the following empirical relation:

$$p = (-T \ln D_{\mathrm{Ca}} - a_2 T - a_3) / a_1,$$

where the $D_{Ca} = Ca^{ol}/Ca^{opx}$ and a_i's are fitted parameters. The prediction error for pressure thus depends on the uncertainty of T and Ca^{ol} as well as the uncertainty of the fitted parameters, so the variance of pressure may be expressed as

$$\sigma_p^2 \approx \left(\frac{\partial p}{\partial T}\right)^2 \sigma_T^2 + \left(\frac{\partial p}{\partial \mathrm{Ca}^{\mathrm{ol}}}\right)^2 \sigma_{\mathrm{Ca}^{\mathrm{ol}}}^2 + \sum_i \left(\frac{\partial p}{\partial a_i}\right)^2 \sigma_{ii}^2 + \sum_i \sum_{j \neq i} \left(\frac{\partial p}{\partial a_i}\right)\left(\frac{\partial p}{\partial a_j}\right)\sigma_{ij},$$

where σ_{ij} is the covariance matrix for the parameters a_i. As KB90 reported only the standard deviation (the square root of the diagonal component of the covariance matrix), we reproduced their linear regression and found that only the parameters a_2 and a_3 are strongly negatively correlated, and in terms of the correlation coefficients ($\rho_{ij} = \sigma_{ij} / (\sqrt{\sigma_{ii}\sigma_{jj}})$), we have $\rho_{12} \approx 0$, ρ_{13}

≈ 0, and $\rho_{23} \approx -1$. With this covariance, the third and fourth terms on the right-hand side are found to nearly cancel out, and they constitute only a few percent of the total variance. The majority of the variance (~80%) is caused by the temperature uncertainty (the first term). Actually, it is not uncommon to observe that the KB90 geobarometer does not yield sensible pressures for spinel peridotites (Strating and Carmichael, 1993; Lee et al., 1996; Wager et al., 1996; O'Reilly et al., 1997; Xu et al., 1998; Laurora et al., 2001). The KB90 was formulated using a relationship of experimental pressure with the partition of Ca between olivine and clinopyroxene, but the majority of their experiments are with garnet peridotites, and the validity of the geobarometer in the spinel stability field is quite uncertain (see O'Reilly et al., 1997 for further critique).

An alternative geobarometry applicable to garnet-free peridotite xenoliths has been proposed based on fluid inclusion (Miller and Richter, 1982; Roedder, 1983). This geobarometry uses the residual pressure or density of fluid inclusion as a depth probe. A number of studies have investigated the depth provenance of peridotite xenoliths using the fluid inclusion geobarometry (Miller and Richter, 1982; Roedder, 1983; Yamamoto et al., 2002; 2007; 2012; Sapienza et al., 2005). During the entrainment of a peridotite xenolith to the Earth's surface, the density of a fluid inclusion can remain unaltered if the plastic deformation of a host mineral is negligible. Note that the effect of diffusive loss of fluid (CO_2) from fluid inclusions in mantle xenoliths is not significant (Yamamoto et al., 2011). The internal pressure of the fluid inclusion is a function of temperature, so if we determine both the two-pyroxene temperature of a xenolith and the density (i.e., residual pressure) of a fluid inclusion, we can estimate the depth where the xenolith was trapped by petit-spot magma.

Minerals in the peridotite xenoliths from petit-spot basalts often have fluid inclusions. According to micro-Raman spectroscopic analyses, the fluid inclusions comprise pure CO_2 (> 99%) (see above section). The fluid (CO_2) densities in the inclusions were determined using micro-Raman densimetry (Yamamoto et al., 2002; Kawakami et al., 2003; Yamamoto and Kagi, 2006; 2008). A delta value, which is a split between two main peaks of Raman spectra of CO_2, can be converted to the density of CO_2 fluid based on an experimental calibration. We analyzed the delta value of the fluid inclusions in the samples. Relevant analytical procedures are described before.

The results of micro-Raman spectroscopic analyses are shown in Table DR3. The maturity of a fluid inclusion is fundamental when estimating the depth provenance of a mantle xenolith (Yamamoto et al., 2011; Bodnar, 2003). An indispensable prerequisite of fluid inclusions for the estimate is that they have negative crystal shape, which reflects the crystal shape of the host mineral and potentially suggest matured inclusions. Among five, relatively large xenoliths, sample 880-2A contains no fluid inclusion with negative crystal shape. The CO_2 inclusions without negative crystal shape in sample 880-2A were disequilibrated with surrounding

temperature and pressure, and they do not reflect the depth provenance. Therefore, the densities of CO_2 in fluid inclusions were obtained from the rest of four peridotite xenoliths, as reported in Table DR3. To obtain precise depth information from residual pressure in a fluid inclusion, even with negative crystal shape, it is important to select a fluid inclusion using *Roedder's Rule* (Roedder, 1984); that is, inclusions are homogeneous, isochoric, and closed systems. When magma traps and entrains a peridotite xenolith to near the sea bottom, a CO_2 inclusion in the peridotite xenolith can principally retain pressure as high as at the time of trapping. The difference between internal pressure of the CO_2 inclusion and outside ambient pressure is manifested as differential stress, which always results in the volume expansion of the CO_2 inclusion induced by elastic or plastic deformation of host minerals. The residual pressure of a CO_2 inclusion is inadequate for use as a depth probe of peridotite xenoliths if the plastic deformation of a host mineral around the CO_2 inclusion occurs intensively during magma transport. Indeed, variations do exist in CO_2 fluid density among different host mineral species; the density generally decreases in the order of orthopyroxene – clinopyroxene >> olivine. The CO_2 densities specific to mineral species in peridotite xenoliths have been frequently reported (Yamamoto and Kagi, 2008; Yamamoto et al., 2002; 2007; 2011; 2012; Sapienza et al., 2005; Schwab and Freisleben, 1988). The low CO_2 fluid density in olivine is attributed to the volume expansion of CO_2 inclusions resulting from the plastic deformation of surrounding crystal lattice in response to differential pressure developed during the ascent of peridotite xenoliths (Andersen and Neumann, 2001; Yamamoto et al., 2002; 2007; 2008; 2011). However, the effect of the volume expansion for pyroxenes is negligible because of their high resistance against plastic deformation (Yamamoto et al., 2008; 2011). Indeed the inclusions with negative crystal shape in pyroxenes show no correlation between CO_2 density and diameter, suggesting that the inclusions have not reequilibrated. In this study, therefore, we adopted CO_2 fluid density in pyroxenes as a depth probe.

The CO_2 density determined in this way varies from 1.16 to 1.21 g/cm^3. The pressure where the xenolith was trapped by petit-spot magma can then be estimated from the intersection of the two-pyroxene temperature, estimated by a pyroxene geothermometer, with isochors in the phase diagram of CO_2 (Fig. 1). The equilibrium pressure of the present xenoliths are estimated as 0.89–1.28 GPa, corresponding to the depth provenance of 26–49 km from sea bottom. The depth of the Gutenberg discontinuity, which is generally regarded as the boundary between the lithosphere and the asthenosphere, is around 80 km below the sea bottom in the northwestern Pacific (Kawakatsu et al., 2009; Shimamura and Asada, 1984). We can thus conclude that these peridotite xenoliths were derived from the middle of the Pacific Plate.

The first issue to be considered is whether the geothermometric data and the density of fluid inclusion were recorded at the same time. In the mantle, both mineral compositions and the density of fluid inclusion can be reequilibrated with changes in surrounding P-T conditions. Timescale for reequilibration may be calculated as follows. When temperature decreases from

1150 to 1050°C, for example, the internal pressure of a CO_2 inclusion should decrease by ~100 MPa. Differential pressure between the internal pressure of a CO_2 inclusion and the ambient pressure is manifested as differential stress, resulting in the volume shrinkage of the CO_2 inclusion because of plastic deformation of host minerals around the CO_2 inclusion. According to the rheological characteristics of orthopyroxene (Mackwell, 1991), the strain rate of orthopyroxene is 4.4×10^{-11} s^{-1} under the differential stress of 100 MPa and the temperature of 1100°C. Applying the strain rate, it takes only ~10 years to deform linearly 1% for orthopyroxene, indicating that the density of fluid inclusion in orthopyroxene would promptly adopt a change in pressure. On the other hand, Ca diffuses for 0.5 mm in clinopyroxene within 1 million years at 1100°C (Zhang et al., 2010). Thus, the geothermometric information recorded in clinopyroxene with 1 mm diameter can be reequilibrated within 1 million years at 1100°C. Even at 1000°C, the pyroxene geothermometer can be reset within several million years. Therefore we believe that the P-T information recorded in the mantle xenoliths reflects the P-T conditions of mature oceanic lithosphere beneath petit-spot volcanoes.

Our depth estimates based on the CO_2 geobarometer are also supported by two independent pieces of information: the mineralogy of the mantle xenoliths and the CO_2 stability condition in the mantle. Regarding the mineralogy, the peridotite xenoliths used in this study are derived from spinel-stability field because they are spinel lherzolite except for sample 2Aa. The pressure of the spinel-to-garnet transition is a function of the fertility of mantle. The transition pressure of the spinel-to-garnet for peridotite is 1.9–2.1 GPa at 800–1100°C (O'Neill, 1981), corresponding to a depth of 58–63 km below the sea bottom. In addition, an upper-limit pressure for the plagioclase-stability field is 0.7–0.8 GPa at 800–1100°C (Borghini et al., 2010), corresponding to a depth of 21–24 km below the sea bottom. That is, a peridotite xenolith derived from the spinel-stability field should have the depth provenance of 21–63 km below the sea bottom. The obtained depth provenance of 26–49 km below the sea bottom for the present spinel-peridotite xenoliths is thus consistent with the petrological constraint. We can obtain the other supporting information from Fig. 1. Assuming a geotherm expected for 140-Ma oceanic lithosphere, no CO_2 inclusion should be detected from olivine in spinel peridotite (Fig. 1). Abundant CO_2 inclusions are, however, observed in olivine of the present samples (Yamamoto et al., 2011) (Fig. DR2), which is consistent with the CO_2 stability condition shown in Fig. 1. Olivine could coexist with CO_2 fluid even on the 140-Ma geotherm, if the pressure is greater than 2 GPa (Fig. 1). The peridotite xenoliths were not derived from such P-T condition because they were originated from the spinel-stability field as described above. Thus the P-T estimates for the peridotite xenoliths are well supported by both mineralogy and the stability condition of CO_2. These observations are a clear proof that the peridotite xenoliths were derived from the oceanic lithosphere whose geotherm is much hotter than expected for 140-Ma oceanic lithosphere.

REFERENCES CITED

Andersen, T., and Neumann, E.-R., 2001, Fluid inclusions in mantle xenoliths. Lithos, v. 55, p. 301–320.

Berkesi, M., Hidas, K., Guzmics, T., Dubessy, J., Bodnar, R.J., Szabó, C., Vajna, B., and Tsunogae, T., 2009, Detection of small amounts of H_2O in CO_2-rich fluid inclusions using Raman spectroscopy. Journal of Raman Spectroscopy, v. 40, p. 1461–1463.

Bodnar, R.J., 2003, Reequilibration of fluid inclusions. in Fluid Inclusions Analysis and Interpretation Short Course of Mineralogical Association of Canada ed. Samson, I., Anderson, A., Marshall, D., v. 32, p. 213–231.

Borghini, G., Fumagalli, P., and Rampone, E., 2010, The stability of plagioclase in the upper mantle: subsolidus experiments on fertile and depleted lherzolite. Journal of Petrology, v. 51, p. 229–254.

Faul, U.H., and Jackson, I., 2005, The seismological signature of temperature and grain size variations in the upper mantle. Earth and Planetary Science Letters, v. 234, p. 119–134.

Fukura, S., Mizukami, T., Odake, S., and Kagi, H., 2006, Factors determining the stability, resolution, and precision of a conventional Raman spectrometer. Applied Spectroscopy, v. 60, p. 946–950.

Kawakami, Y., Yamamoto, J., and Kagi, H., 2003, Micro-Raman densimeter for CO_2 inclusions in mantle-derived minerals. Applied Spectroscopy, v. 57, p. 1333–1339.

Kawakatsu, H. Kumar, P. Takei, Y. Shinohara, M. Kanazawa, T., Araki, E., and Suyehiro, K., 2009, Seismic evidence for sharp lithosphere-asthenosphere boundaries of oceanic plates. Science, v. 324, p. 499–502.

Köhler, T., and Brey, G.P., 1990, Calcium exchange between olivine and clinopyroxene calibrated as a geothermobarometer for natural peridotites from 2 to 60 kb with applications. Geochimica et Cosmochimica Acta, v. 54, p. 2375–2388.

Laurora, A., Mazzucchelli, M., Rivalenti, G., Vannucci, R., Zanetti, A., Barbieri, M.A., and Cingolani, C.A., 2001, Metasomatism and melting in carbonated peridotite xenoliths from the mantle wedge: The Gobernador Gregores case (Southern Patagonia). Journal of Petrology, v. 42, p. 69–87.

Lee, D.C., Halliday, A.N., Davies, G.R., Essene, E.J., Fitton, J.G., and Temdjim, R., 1996, Melt enrichment of shallow depleted mantle: A detailed petrological trace element and isotopic study of mantle-derived xenoliths and megacrysts from Cameroon line. Journal of Petrology, v. 37, p. 415–441.

Mackwell, S.J., 1991, High-temperature rheology of enstatite: implications for creep in the mantle. Geophysical Research Letters, v. 18, p. 2027-2030.

Miller, C., and Richter, W., 1982, Solid and fluid phases in lherzolite and pyroxenite inclusions from the Hoggar central Sahara. Geochemical Journal, v. 16, p. 263–277.

O'Neill, H.St.C., 1981, The transition between spinel lherzolite and garnet lherzolite and its use as a geobarometer. Contributions to Mineralogy and Petrology, v. 77, p. 185–194.

O'Reilly, S.Y., Chen, D., Griffin, W.L., and Ryan, C.G., 1997, Minor elements in olivine from spinel lherzolite xenoliths: implications for thermobarometry. Mineralogical Magazine, v. 61, p. 257–269.

Pitzer, K.S., and Sterner, S.M., 1994, Equations of state valid continuously from zero to extreme pressures for H_2O and CO_2. The Journal of Chemical Physics, v. 101, p. 3111–3116.

Putirka, K., 2008, Thermometers and barometers for volcanic systems. Review in Mineralogy and Geochemistry, v. 69, p. 61–120.

Roedder, E., 1983, Geobarometry of ultramafic xenoliths from Loihi Seamount Hawaii on the basis of CO_2 inclusions in olivine. Earth and Planetary Science Letters, v. 66, p. 369–379.

Roedder, E., 1984, Fluid Inclusions. Mineral Soc Am Washington DC Rev. Mineral. 12, pp 646.

Sapienza, G., Hilton, D.R., Scribano, V., 2005, Helium isotopes in peridotite mineral phases from Hyblean Plateau xenoliths (south-eastern Sicily, Italy). Chemical Geology, v. 219, p. 115–129.

Schwab, R.G., and Freisleben, B., 1988, Fluid CO_2 inclusions in olivine and pyroxene and their behaviour under high pressure and temperature conditions. Bulletin of Mineralogy, v. 111, p. 297–306.

Shimamura, H., and Asada, T., 1984, Velocity anisotropy extending over the entire depth of the oceanic lithosphere. In: Hilde, T.W.C. & Uyeda, S. (Eds) Geodynamics Sereis v. 11, p. 121–125.

Strating, E.H.H., and Carmichael, I.S.E., 1993, Subsolidus emplacement of mantle peridotites during incipient oceanic rifting and opening of the Mesozoic Tethys (Voltri massif NW Italy). Journal of Petrology, v. 34, p. 901–927.

Taneja, R., O'Neill, C., Lackie, M., Rushmer, T., Schmidt, P., and Jourdan, F., 2014, $^{40}Ar/^{39}Ar$ geochronology and the paleoposition of Christmas Island (Australia), Northeast Indian Ocean. Gondwana Research, in press.

Uenzelmann-Neben, G., Schmidt, D.N., Niessen, F., and Stein, R., 2012, Intraplate volcanism off South Greenland: caused by glacial rebound? Geophysical Journal International, 190, 1–7.

Valentine, G., and Hirano, N., 2010, Mechanisms of low-flux intraplate volcanic fields - Basin and Range (North America) and Northwest Pacific Ocean. Geology, 38, 55–58.

Wager, C., Deloule, E., and Mokhtari, A., 1996, Richterite-bearing peridotites and MARID-type inclusions in lavas from North Eastern Morocco: Mineralogy and D/H isotopic studies. Contributions to Mineralogy and Petrology, v. 124, p. 406–421.

Wells, P.R.A., 1977, Pyroxene thermometry in simple and complex systems. Contributions to Mineralogy and Petrology, v. 62, p. 129–139.

Xu, Y.G., Menzies, M.A., Bodinier, J.L., Bedini, R.M., Vroon, P., and Mercier, J.-C.C., 1998, Melt percolation and reaction atop a plume: evidence from the poikiloblastic peridotite xenoliths from Boree (Massif Central France). Contributions to Mineralogy and Petrology, v. 132, p. 65–84.

Yamamoto, J., and Kagi, H., 2006, Extended micro-Raman densimeter for CO_2 applicable to mantle-originated fluid inclusions. Chemistry Letters, v. 35, p. 610–611.

Yamamoto, J., and Kagi, H., 2008, Application of micro-Raman densimeter for CO_2 fluid inclusions: a probe for elastic strengths of mantle minerals. European Journal of Mineralogy, v. 20, p. 529–535.

Yamamoto, J., Kagi, H., Kaneoka, I., Lai, Y., Prikhod'ko, V.S., and Arai, S., 2002, Fossil pressures of fluid inclusions in mantle xenoliths exhibiting rheology of mantle minerals: implications for the geobarometry of mantle minerals using micro Raman spectroscopy. Earth and Planetary Science Letters, v. 198, p. 511–519.

Yamamoto, J., Kagi, H., Kawakami, Y., Hirano, N., and Nakamura, M., 2007, Paleo-Moho depth determined from the pressure of CO_2 fluid inclusions: Raman spectroscopic barometry of mantle- and crust-derived rocks. Earth and Planetary Science Letters, 253, p. 369–377.

Yamamoto, J., Ando, J., Kagi, H., Inoue, T., Yamada, A., Yamazaki, D., and Irifune, T., 2008, In-situ strength measurements on natural upper-mantle minerals. Physics and Chemistry of Minerals, v. 35, p. 249–257.

Yamamoto, J., Hirano, N., Abe, N., and Hanyu, T., 2009, Noble gas isotopic compositions of mantle xenoliths from northwestern Pacific lithosphere. Chemical Geology, v. 268, p. 313–323.

Yamamoto, J., Otsuka, K., Ohfuji, H., Ishibashi, H., Hirano, N., and Kagi, H., 2011, Retentivity of CO_2 in fluid inclusions in mantle minerals. European Journal of Mineralogy, v. 23, p. 805–815.

Yamamoto, J., Nishimura, K., Ishibashi, H., Kagi, H., Arai, S., and Prikhod'ko, V.S., 2012, Thermal structure beneath Far Eastern Russia inferred from geothermobarometric analyses of mantle xenoliths: direct evidence for high geothermal gradient in backarc lithosphere. Tectonophysics, v. 554–557, p. 74–82.

Zhang, X., Ganguly, J., and Ito, M., 2010, Ca-Mg diffusion in diopside: tracer and chemical inter-diffusion coefficients. Contributions to Mineralogy and Petrology, v. 159, p. 175-186.

FIGURE CAPTIONS

Figure DR1. Map of the northwestern Pacific Ocean. Petit-spot volcanoes erupted at the oceanward root of outer rise where subducting ocean plate begins to bend. Taking eruption age of the volcano containing 6K#880 into consideration, it erupted at a similar place to that containing 6K#878.

Figure DR2. Photomicrographs of thin slabs of sample 2D. An array of liquid CO_2 inclusions in (a) an orthopyroxene and (b) an olivine. These have negative crystal shape and show no correlation between CO_2 density and diameter, suggesting that the inclusions have not reequilibrated.

Figure DR3. Raman spectra of a fluid inclusion in an olivine of sample 2D measured at (a) room temperature and (b) 150°C using a Linkam THMS600 heating/cooling stage. Raman spectra were obtained using a micro-Raman spectrum analyzing system at the Hokkaido University Museum. The samples were excited with an Ar ion laser (514.5 nm, 43 Series, CVI Melles Griot LLC). Raman scattering light was guided into a spectrometer (Acton SP-2750, Princeton Instruments Inc.) and detected using a CCD camera (1650 × 200 pixels, iVac; Andor Technology PLC). The Raman spectra were collected for 60 seconds with a laser power of 18 mW at sample.

Figure DR1

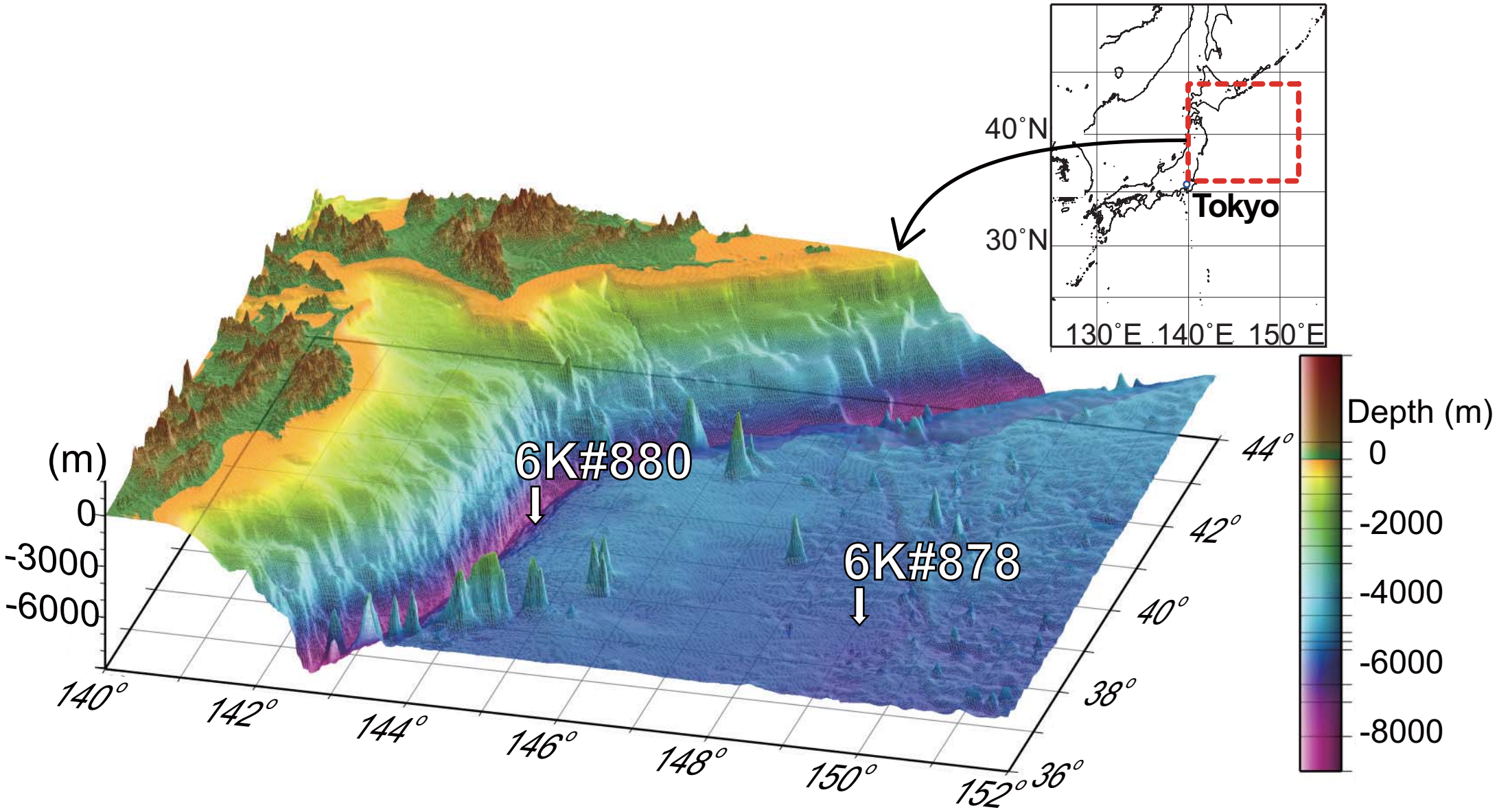
40˚N
30˚N
Tokyo
130˚E 140˚E 150˚E
(m)
0
-3000
-6000
6K#880
6K#878
140°
142°
144°
146°
148°
150°
152°
36°
38°
40°
42°
44°
Depth (m)
0
-2000
-4000
-6000
-8000

Figure DR2

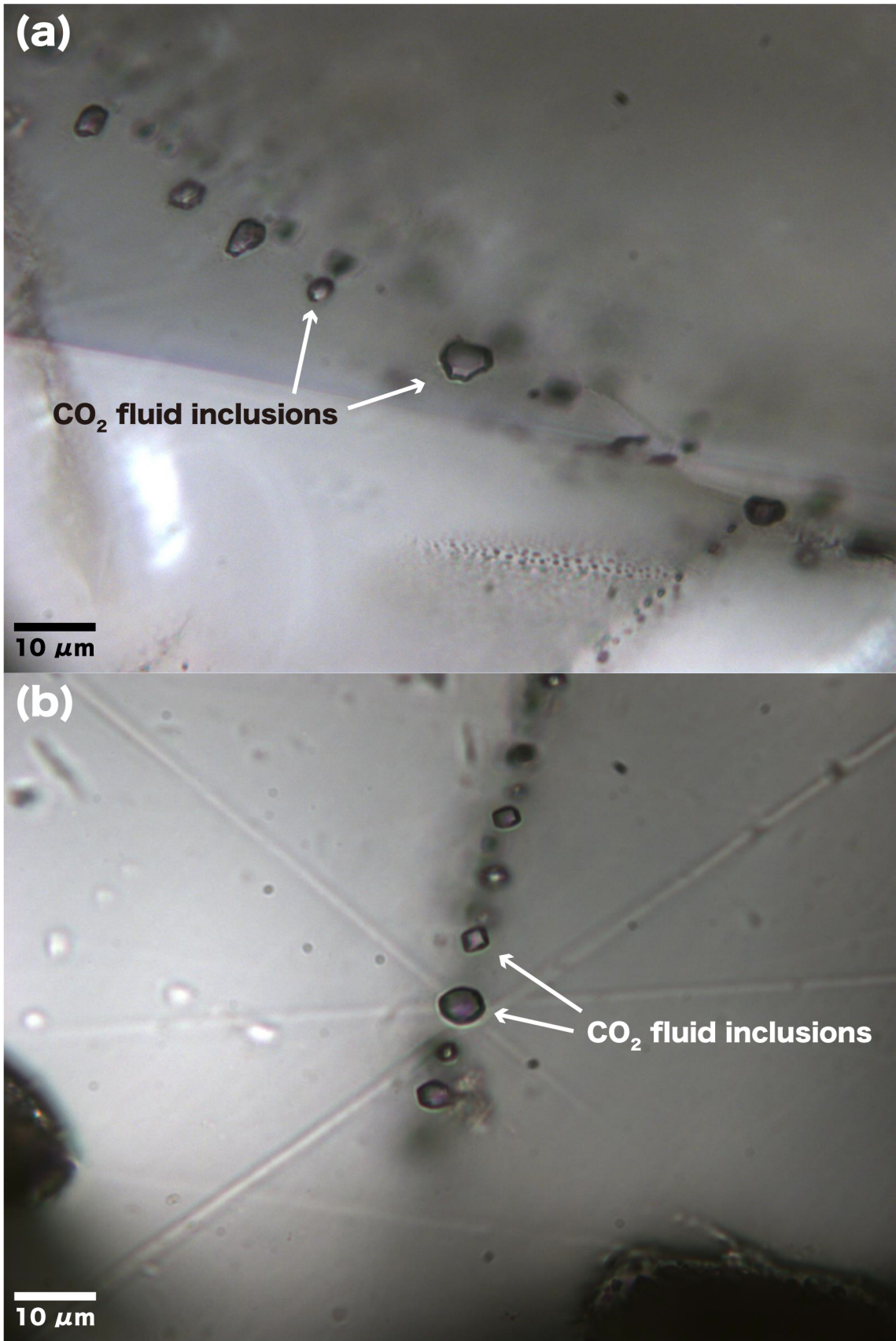

Figure DR3

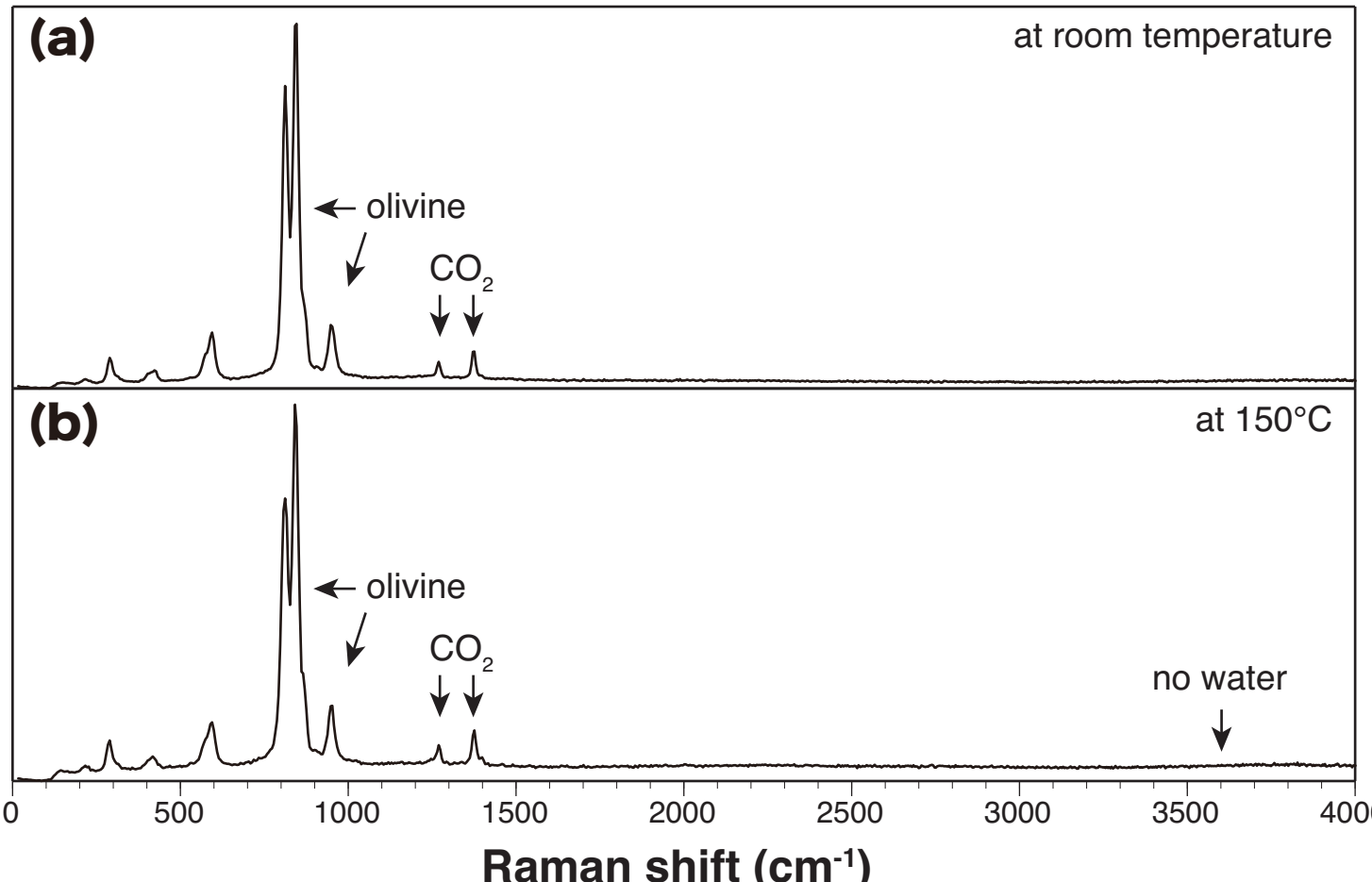
(a)
at room temperature
olivine
CO2
(b)
at 150°C
olivine
CO2
no water
0
500
1000
1500
2000
2500
3000
3500
4000
Raman shift (cm-1)

Table DR1. Average compositions of core part of minerals

Dredge No.	6K#878			6K#878			6K#878			6K#880			
Samples	2As			2Al			2Aa			2D			
Rocktype	spinel-lherzolite xenolith			spinel-lherzolite xenolith			lherzolite xenolith			spinel-lherzolite xenolith			
Mineral	olivine	opx	cpx	olivine	opx	cpx	olivine	opx	cpx	olivine	opx	cpx	spinel
Mg#	92.76	91.87	92.40	90.95	89.53	91.67	89.72	90.07	94.08	91.40	91.65	91.04	73.48
Cr#													21.86
SiO_2	42.70	55.90	53.27	42.32	55.06	52.31	41.23	55.92	53.84	41.56	56.08	53.35	0.23
TiO_2	0.02	0.09	0.21	0.00	0.10	0.52	0.01	0.09	0.46	0.02	0.12	0.26	0.94
Al_2O_3	0.01	2.16	3.02	0.00	4.76	6.09	0.00	4.89	6.23	0.05	3.21	4.01	45.85
Cr_2O_3	0.01	0.46	1.12	0.00	0.32	0.63	0.01	0.36	0.55	0.05	0.85	1.65	19.07
FeO	7.14	5.26	2.42	8.91	6.89	2.36	9.78	6.31	1.73	8.35	5.33	3.01	12.58
MnO	0.09	0.12	0.07	0.12	0.06	0.04	0.13	0.13	0.08	0.11	0.12	0.09	0.22
MgO	51.30	33.37	16.51	50.22	33.03	14.58	47.86	32.11	15.43	49.78	32.79	17.13	19.53
CaO	0.04	0.59	20.54	0.02	0.31	21.67	0.02	0.28	19.23	0.10	1.10	18.58	0.01
Na_2O	0.03	0.06	1.15	0.00	0.05	1.75	0.01	0.04	1.78	0.01	0.12	1.13	0.00
K_2O	0.02	0.01	0.02	0.01	0.00	0.00	0.01	0.02	0.02	0.01	0.01	0.00	0.01
NiO	0.25	0.07	0.04	0.28	0.09	0.04	0.33	0.06	0.03	0.39	0.11	0.06	0.31
Total	101.61	98.11	98.36	101.90	100.67	99.99	99.41	100.21	99.39	100.40	99.84	99.26	98.72
T [˚C]	990	±44		771	±58		1030	±55		1129	±30		
K_D (Fe-Mg)*	0.93			0.78			0.57			1.08			

Multiple points in the core of a single grain of each mineral species were analyzed. Equilibrium temperatures (T) were estimated by two-pyroxene geothermometer of Wells (1977). opx, orthopyroxene; cpx, clinopyroxene. * K_D (Fe-Mg) is $(X^{cpx}_{Fe}/X^{cpx}_{Mg})/(X^{opx}_{Fe}/X^{opx}_{Mg})$ where X^j_i refers to the mole fraction of component *i* in phase *j*. Major element compositions were analyzed using an electron probe microanalyzer (JEOL JXA-8800) at Tokyo Institute of Technology. The contents of CaO, MnO and NiO in olivine were analyzed using an accelerating voltage of 25 kV and a beam current of 20 nA. For the other elements, analyses were performed under an accelerating voltage of 15 kV and a beam current of 12 nA. Integrated times for measurements were 200s for most elements and 20s for Na and K.

Table DR2. Average compositions of rim part of minerals

Dredge No.	6K#878			6K#878			6K#878			6K#880			
Samples	2As			2Al			2Aa			2D			
Rocktype	spinel-lherzolite xenolith			spinel-lherzolite xenolith			lherzolite xenolith			spinel-lherzolite xenolith			
Mineral	olivine	opx	cpx	olivine	opx	cpx	olivine	opx	cpx	olivine	opx	cpx	spinel
Mg#	92.73	91.78	92.47	90.92	89.63	91.80	89.77	90.18	94.15	91.33	91.55	90.99	73.69
Cr#													20.09
SiO_2	42.84	55.84	53.21	41.52	55.02	52.12	40.42	56.00	54.16	41.48	56.01	53.32	0.19
TiO_2	0.03	0.06	0.21	0.01	0.10	0.52	0.02	0.09	0.41	0.01	0.14	0.25	0.92
Al_2O_3	0.02	2.17	3.02	0.00	4.44	6.25	0.00	4.92	6.30	0.05	3.35	3.98	47.07
Cr_2O_3	0.00	0.47	1.15	0.00	0.29	0.70	0.01	0.35	0.55	0.06	0.86	1.63	17.56
FeO	7.17	5.33	2.38	8.85	6.82	2.31	9.63	6.27	1.72	8.46	5.38	3.03	12.83
MnO	0.11	0.13	0.10	0.13	0.13	0.03	0.11	0.15	0.09	0.12	0.11	0.10	0.16
MgO	51.26	33.41	16.40	49.73	33.09	14.49	47.42	32.28	15.55	50.00	32.77	17.17	20.16
CaO	0.03	0.56	20.48	0.00	0.33	21.40	0.01	0.30	19.30	0.09	1.16	18.63	0.00
Na_2O	0.01	0.06	1.17	0.00	0.04	1.75	0.01	0.03	1.80	0.01	0.12	1.18	0.00
K_2O	0.01	0.01	0.02	0.00	0.00	0.00	0.02	0.02	0.02	0.01	0.01	0.01	0.00
NiO	0.23	0.08	0.04	0.30	0.06	0.05	0.32	0.06	0.04	0.38	0.11	0.06	0.31
Total	101.70	98.14	98.18	100.56	100.34	99.64	97.97	100.48	99.95	99.94	100.02	99.36	99.20
T [˚C]	987	±47		802	±151		1032	±59		1125	±35		
K_D (Fe-Mg)*	0.91			0.77			0.57			1.07			

Multiple points in the rim of a single grain of each mineral species were analyzed. Analytical conditions were the same as those of Table A1.

Table DR3. Results of geothermobarometry for petit-spot mantle xenoliths

Dredge No.	6K#878	6K#878	6K#878	6K#880
Samples	2As	2Al	2Aa	2D
Sites	Yukawa Knolls	Yukawa Knolls	Yukawa Knolls	Kaiko knolls
Rock type	spinel-lherzolite	spinel-lherzolite	lherzolite	spinel-lherzolite
CO_2 density (g/cm^3)*	1.155 ± 0.006	1.156 ± 0.013	1.167 ± 0.007	1.205 ± 0.010
T (°C)†	990 ± 44	771 ± 58	1030 ± 55	1129 ± 30
P_FI (GPa)§	1.061 ± 0.049	0.892 ± 0.077	1.123 ± 0.061	1.311 ± 0.055
P_KB90 (GPa)#	2.7 ± 0.6	1.9 ± 1.0	4.3 ± 0.9	2.0 ± 0.6
P_maximum (GPa)**	2.1	1.9	2.1	2.2

*Errors are derived only from reproducibility of repeated analyses of delta value.
†Equilibrium temperature (T) are from Table A1.
§Equilibrium pressure (P_FI) were calculated using an equation of state for CO_2 (Pitzer and Sterner, 1994).
#Equilibrium pressure (P_KB90) were estimated using a geobarometer of Köhler and Brey (1990) and data of Table A1.
**Maximum pressure estimate based on the stability of spinel peridotite by considering Fo value of each sample and Cr# of spinel in sample 2D. T, P_KB90 and P_maximum of sample 880-2A are 1035 ± 81°C, 4.5 ± 1.1 GPa and 2.1 GPa, respectively.
Latitude and longitude of Yukawa and Kaiko knolls are respectively 37°37.60’ N, 149°30.50’ E and 39° 23.78’ N, 144° 26.30’ W.